

The Arf GAP Asap promotes Arf1 function at the Golgi for cleavage furrow biosynthesis in *Drosophila*

Francisco F. Rodrigues, Wei Shao, and Tony J. C. Harris*

Department of Cell and Systems Biology, University of Toronto, Toronto, ON M5S 3G5, Canada

ABSTRACT Biosynthetic traffic from the Golgi drives plasma membrane growth. For *Drosophila* embryo cleavage, this growth is rapid but regulated for cycles of furrow ingression and regression. The highly conserved small G protein Arf1 organizes Golgi trafficking. Arf1 is activated by guanine nucleotide exchange factors, but essential roles for Arf1 GTPase-activating proteins (GAPs) are less clear. We report that the conserved Arf GAP Asap is required for cleavage furrow ingression in the early embryo. Because Asap can affect multiple subcellular processes, we used genetic approaches to dissect its primary effect. Our data argue against cytoskeletal or endocytic involvement and reveal a common role for Asap and Arf1 in Golgi organization. Although Asap lacked Golgi enrichment, it was necessary and sufficient for Arf1 accumulation at the Golgi, and a conserved Arf1-Asap binding site was required for Golgi organization and output. Of note, Asap relocalized to the nuclear region at metaphase, a shift that coincided with subtle Golgi reorganization preceding cleavage furrow regression. We conclude that Asap is essential for Arf1 to function at the Golgi for cleavage furrow biosynthesis. Asap may recycle Arf1 to the Golgi from post-Golgi membranes, providing optimal Golgi output for specific stages of the cell cycle.

Monitoring Editor
Richard Fehon
University of Chicago

Received: May 4, 2016
Revised: Jul 6, 2016
Accepted: Aug 11, 2016

INTRODUCTION

The highly conserved small G protein Arf1 plays a ubiquitous role in regulating the flow of materials through the Golgi apparatus. Guanine nucleotide exchange factors (GEFs) produce Arf1-GTP, which induces two forms of vesicle budding from the Golgi. Arf1-GTP recruits the COPI coat for retrograde trafficking through the Golgi and from the *cis*-Golgi to the endoplasmic reticulum (ER), and its interaction with the clathrin adaptor AP-1 complex organizes budding from the *trans*-Golgi network (TGN) to other membrane

systems and the plasma membrane (PM; Lorente-Rodriguez and Barlowe, 2011; Guo *et al.*, 2014; Papanikou and Glick, 2014). GTPase-activating proteins (GAPs) convert Arf1-GTP into Arf1-GDP and thus reverse the direct effect of GEFs (Gillingham and Munro, 2007; Donaldson and Jackson, 2011). However, GAPs are not simply off switches. Arf GAPs are typically multidomain proteins and couple their GAP activity with other molecular interactions to coordinate vesicle maturation during biosynthesis (Gillingham and Munro, 2007; Spang *et al.*, 2010; Donaldson and Jackson, 2011; East and Kahn, 2011).

Although biochemical and subcellular analyses have identified specific mechanisms of action for Arf1 GAPs at the Golgi, loss-of-function studies indicate that these mechanisms are redundant for cell viability. This redundancy was first discovered in single- and double-mutant analyses of the yeast Arf GAPs Gsc1 and Glo3, which act at the *cis*-Golgi (Poon *et al.*, 1999), and was then found among three Arf GAPs in mammalian cell culture; ARFGAP1 (homologue of Gsc1) and ARFGAP2 and ARFGAP3 (homologues of Glo3; Frigerio *et al.*, 2007). Redundancy may also explain the viability of *Drosophila* mutants for *Gap69C* (homologue of Gsc1/ARFGAP1; Frolov and Alatortsev, 2001) and is evident for homologues of Glo3 in *Arabidopsis* (Min *et al.*, 2013). These Arf1 GAPs may thus play redundant, constitutive roles for Golgi function. Here we

This article was published online ahead of print in MBoC in Press (<http://www.molbiolcell.org/cgi/doi/10.1091/mbc.E16-05-0272>) on August 17, 2016.

None of the authors has any competing interests.

*Address correspondence to: Tony J. C. Harris (tony.harris@utoronto.ca).

Abbreviations used: Amph, amphiphysin; Asap, ArfGAP with SH3 domain, ankyrin repeat, and PH domain; BDSC, Bloomington *Drosophila* Stock Center; DSHB, Developmental Studies Hybridoma Bank; ER, endoplasmic reticulum; GAP, GTPase-activating protein; GEF, guanine nucleotide exchange factor; LqfR, Liquid facets-related; MTD, Maternal Triple Driver; pH3, phospho-histone H3; PM, plasma membrane; PGC, primordial germ cell; shRNA, short hairpin RNA; TGN, *trans*-Golgi network.

© 2016 Rodrigues *et al.* This article is distributed by The American Society for Cell Biology under license from the author(s). Two months after publication it is available to the public under an Attribution-Noncommercial-Share Alike 3.0 Unported Creative Commons License (<http://creativecommons.org/licenses/by-nc-sa/3.0>).

"ASCB®," "The American Society for Cell Biology®," and "Molecular Biology of the Cell®" are registered trademarks of The American Society for Cell Biology.

report an alternate paradigm in which a distinct Arf GAP, Asap (ArfGAP with SH3 domain, ankyrin repeat, and PH domain), is essential for general Golgi activity.

Arf1 is the preferred substrate of ASAP-1 (Asap in *Drosophila*; Furman et al., 2002). In mammalian cell culture, ASAP-1 localizes at the PM and promotes cytoskeletal remodeling and focal adhesion activity for cell spreading and protrusion (Randazzo et al.,

2000; Furman et al., 2002; Liu et al., 2005; Bharti et al., 2007). In the developing *Drosophila* eye, Asap localizes to the PM and affects cell arrangement (Johnson et al., 2011). Asap is also found at the PM of the *Drosophila* embryonic ectoderm and contributes to epithelial development (Shao et al., 2010). In frog photoreceptor cells, ASAP-1 has a distinct role at the TGN, where it acts with Arf4 and Rab small G proteins for the targeting of rhodopsin to cilia (Mazelova et al., 2009; Wang et al., 2012). Overall these studies suggest that ASAP-1/Asap influences both the PM and the Golgi, although the extent of its Golgi activities is unknown. Similarly, Arf1 promotes endocytosis at the PM in addition to its Golgi functions (Donaldson and Jackson, 2011).

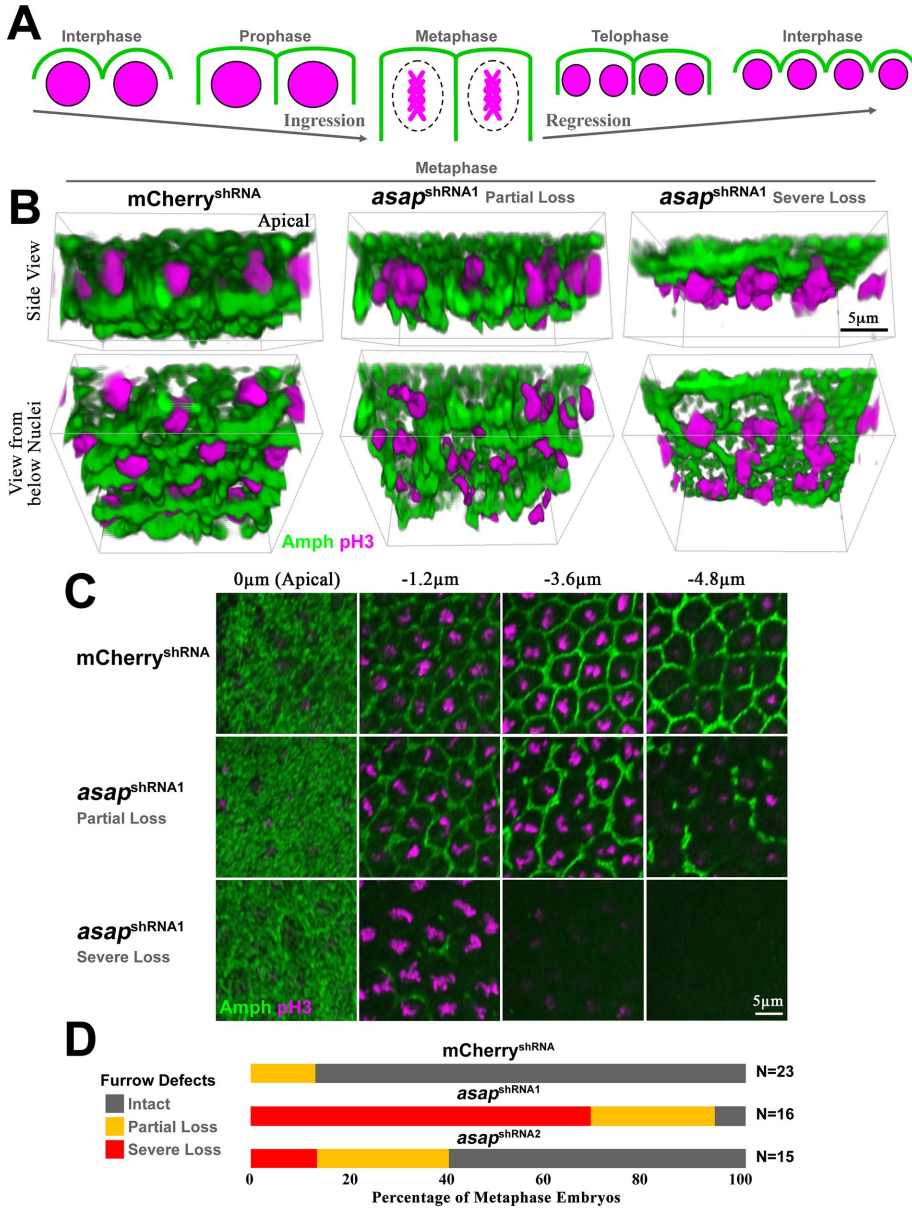


FIGURE 1: Asap is necessary for early-embryo cleavage furrows. (A) Schematic of PM furrow behavior (green) during the peripheral nuclear divisions of the syncytial *Drosophila* embryo. Two nuclei (purple) are shown to divide into four nuclei in a small cross-section of the embryo periphery. Note the furrow ingression from interphase to metaphase, the maximum furrow depth at metaphase, and the furrow regression from metaphase to the following interphase. (B) 3D reconstructions of ~10–12 peripheral cell compartments in syncytial *Drosophila* embryos at metaphase, when furrows are normally deepest. Furrows marked with Amph (green) and metaphase chromosomes detected with pH3 (magenta). A control mCherry^{shRNA} embryo with intact furrows is compared with *asap*^{shRNA1} embryos with partial or severe furrow loss. (C) xy-sections from the embryo surface to below the nuclei for the embryos shown in B. (D) Quantifications of the furrow structure of control and Asap RNAi embryos (two distinct *asap* shRNAs were analyzed). N, number of metaphase embryos counted for each genotype (compiled from two or more experiments, each with similar results). Constructs were expressed maternally with *matα*TubGAL4::VP16.

Membrane trafficking and cytoskeletal activities are central to cleavage of the early *Drosophila* embryo. The early embryo is a syncytium. The first nuclear divisions occur deep within the embryo, and then most nuclei migrate to the embryo periphery just beneath the PM (Foe and Alberts, 1983; Sullivan and Theurkauf, 1995). As part of this migration, a centrosomal microtubule array individualizes an endomembrane system for each nucleus (Frescas et al., 2006). In addition, overlap between neighboring microtubule networks dictates where furrows ingress from the embryo surface (Sisson et al., 1999). For each synchronous nuclear division cycle, these furrows are temporary; they form during interphase, reach a maximum depth at metaphase to anchor and separate mitotic spindles, and then regress (Foe and Alberts, 1983; Sullivan and Theurkauf, 1995; Sisson et al., 1999; Figure 1A). This cycle repeats several times to produce ~6000 nuclei, after which full cellularization forms the blastoderm (Mazumdar and Mazumdar, 2002; Lecuit, 2004; Lee and Harris, 2014). For full cellularization, membrane biosynthesis from the Golgi has a well-documented role in fuelling the ~25-fold PM growth required for the process (Lecuit and Wieschaus, 2000; Sisson et al., 2000; Frescas et al., 2006). Similarly, the repeated furrow ingressions of the preceding nuclear divisions require Arf1 (Lee et al., 2015a) and exocytic machinery (Holly et al., 2015; Mavor et al., 2016). This outward trafficking is coupled with actin-based cytoskeletal networks and PM recycling routes to support furrow ingression (Lee and Harris, 2014). How furrows regress with each division is less clear and requires greater understanding of ingression mechanisms and how they could be reversed.

We discovered an essential role for Asap in forming early-embryo cleavage furrows. Our experiments revealed that Asap is necessary and sufficient for Arf1

accumulation at the Golgi and that both proteins, as well as their conserved binding site, are required for proper Golgi structure and general output to the PM. Remarkably, Asap translocates to the nuclear region before each cycle of furrow regression, a shift accompanied by altered Golgi structure. Thus an Asap-Arf1-Golgi pathway appears to fuel cleavage furrow ingression and may be regulated by Asap sequestration during the cell cycle.

RESULTS

Asap is required for cleavage furrow ingression

To perturb Asap in the early embryo, we pursued a maternal RNA interference (RNAi) strategy. We designed short hairpin RNA (shRNA) constructs that target distinct sequences, expressed them in the female germline, and examined embryos produced from these females. To assess cleavage furrows, we stained embryos with amphiphysin (Amph), a PM marker enriched at furrow tips, and phospho-histone H3 (pH3), a marker of mitotic chromosomes that allows selection of embryos at metaphase, when furrow ingression is greatest (Foe and Alberts, 1983; Sullivan and Theurkauf, 1995; Sisson et al., 1999; Figure 1A). Control mCherry^{shRNA} embryos displayed full furrow ingression at metaphase (Figure 1, B–D), whereas two distinct *asap* shRNA constructs induced furrow loss, *asap*^{shRNA1} more severely than *asap*^{shRNA2} (Figure 1, B–D). Consistent with other reports (e.g., Holly et al., 2015), embryos with furrow loss often displayed abnormally arranged and fused nuclei (see later discussion of Figure 5), suggesting a failure to separate mitotic spindles in the absence of furrows. However, at the earliest peripheral nuclear division cycle, Asap RNAi embryos were indistinguishable from controls (Supplemental Figure S1), indicating that early mitoses deep within the embryo were unaffected by Asap depletion. The stronger *asap* shRNA, *asap*^{shRNA1}, also induced partial female infertility (Table 1). Coexpression of an Asap–green fluorescent protein (GFP) construct with control and *asap* shRNA constructs confirmed that Asap protein levels were substantially reduced by *asap*^{shRNA1} and to a lesser extent by *asap*^{shRNA2} (unpublished data), consistent with their relative effects on furrows.

To examine what step of furrow formation is disrupted with *asap* RNAi, we performed live imaging of a PM marker in individual embryos over several cleavage cycles. At interphase, *asap* RNAi embryos could form PM caps similar to controls, but these caps became abnormally scattered over several division cycles (Figure 2; compare apical surface sections). After interphase, *asap* RNAi

embryos typically failed to ingress furrows from the PM caps (Figure 2, side views; four of six embryos formed no furrows, and two of six embryos showed partial ingression), in contrast to control embryos displaying furrow ingression (Figure 2, arrowheads; four of four embryos). Overall these results show that Asap is required specifically for cleavage furrow ingression in the early embryo.

Asap exists at multiple subcellular sites and relocates during the cell cycle

To understand how Asap promotes cleavage furrows, we imaged GFP-tagged Asap constructs (Shao et al., 2010), as well as antibody staining for endogenous Asap (Johnson et al., 2011). Previously these probes revealed Asap localization to cell–cell junctions in later *Drosophila* tissues (Shao et al., 2010; Johnson et al., 2011). However, Asap antibody staining was at background levels in the early embryo (unpublished data), suggesting a relatively low expression level, a disperse protein distribution, or a masked antibody epitope. Thus we analyzed overexpressed, GFP-tagged Asap constructs in the early embryo and assessed whether their localization was relevant to endogenous Asap by comparing their distributions to that of antibody staining in slightly later embryos.

Live imaging of GFP-Asap (N-terminally tagged) revealed a dramatic relocation of the protein during the cleavage cycles of the early embryo. During interphase, GFP-Asap localized in a punctate distribution over the PM (Figure 3A, blue arrows) and to early PM furrows (Figure 3A, white arrows), with a cytoplasmic pool apparent by nuclear exclusion (Figure 3A, asterisks). As the nuclear envelope broke down just before metaphase, GFP-Asap lost its PM association and nuclear exclusion and quickly became enriched in the nuclear region relative to the surrounding cytoplasm (Figure 3A, yellow arrows). This nuclear localization was gradually lost from metaphase to telophase, and the protein relocated to the PM by the next interphase (unpublished data). Live imaging of Asap-GFP (C-terminally tagged) revealed similar patterns of PM localization and nuclear exclusion at interphase followed by nuclear enrichment at prometaphase (Supplemental Figure S2)

Next we compared GFP-Asap with several membrane and cytoskeletal markers. At interphase, GFP-Asap puncta colocalized with actin-rich PM protrusions over the apical surface and to early furrows of the cell compartments (Figure 3, B, arrows, and C, side view). Intracellularly, GFP-Asap was distributed as weaker puncta throughout the cytoplasm, with patchy enrichment around the nuclear periphery but with no specific overlap with AP-1–positive Golgi elements (Figure 3C) and with nuclear exclusion (Figure 3C, asterisk). At prometaphase, GFP-Asap became enriched within the nuclear region but was excluded from condensed chromosomes (Figure 3D, arrow, inset), a pattern resembling that reported for markers of the nucleoplasm (Trieselmann and Wilde, 2002) and nuclear matrix (Walker et al., 2000).

To test whether endogenous Asap displayed similar localization patterns, we analyzed antibody staining in the ectoderm of embryos 2–3 h after completion of the syncytial divisions. In the ectoderm of stage 8–9 embryos, Asap antibody staining revealed strong PM localization and weaker cytoplasmic localization, with no enrichment at AP-1–positive Golgi elements (Figure 3E). At interphase, endogenous Asap displayed nuclear exclusion (Figure 3F, asterisk). At metaphase, the staining was enriched within the nuclear region surrounding condensed chromosomes (Figure 3F, arrow). Together these probes suggest that Asap could function at the PM or within the cytoplasm, and no specific associations with the Golgi were detected. In addition, all three probes revealed a relocation of Asap to the nuclear region at prometaphase.

UAS constructs	Expression level	Female infertility
<i>asap</i> ^{shRNA1}	High ^a	Full
	Medium ^b	Strong
<i>asap</i> ^{shRNA2}	High	Undetectable
<i>arf1</i> ^{shRNA2} + GFP	Medium	Strong
<i>arf1</i> ^{shRNA2} + <i>arf1</i> ^[N52A]	Medium	Undetectable
<i>arf1</i> ^{shRNA2} + <i>arf1</i> ^[I46D]	Medium	Strong
<i>arf1</i> ^[N52A]	High	Undetectable
	Medium	Undetectable
<i>arf1</i> ^[I46D]	High	Strong
	Medium	Partial

^aExpression with Maternal Triple Driver.

^bExpression with *matαTubGAL4::VP16*.

TABLE 1: Perturbations of Asap or Arf1 affecting female fertility.

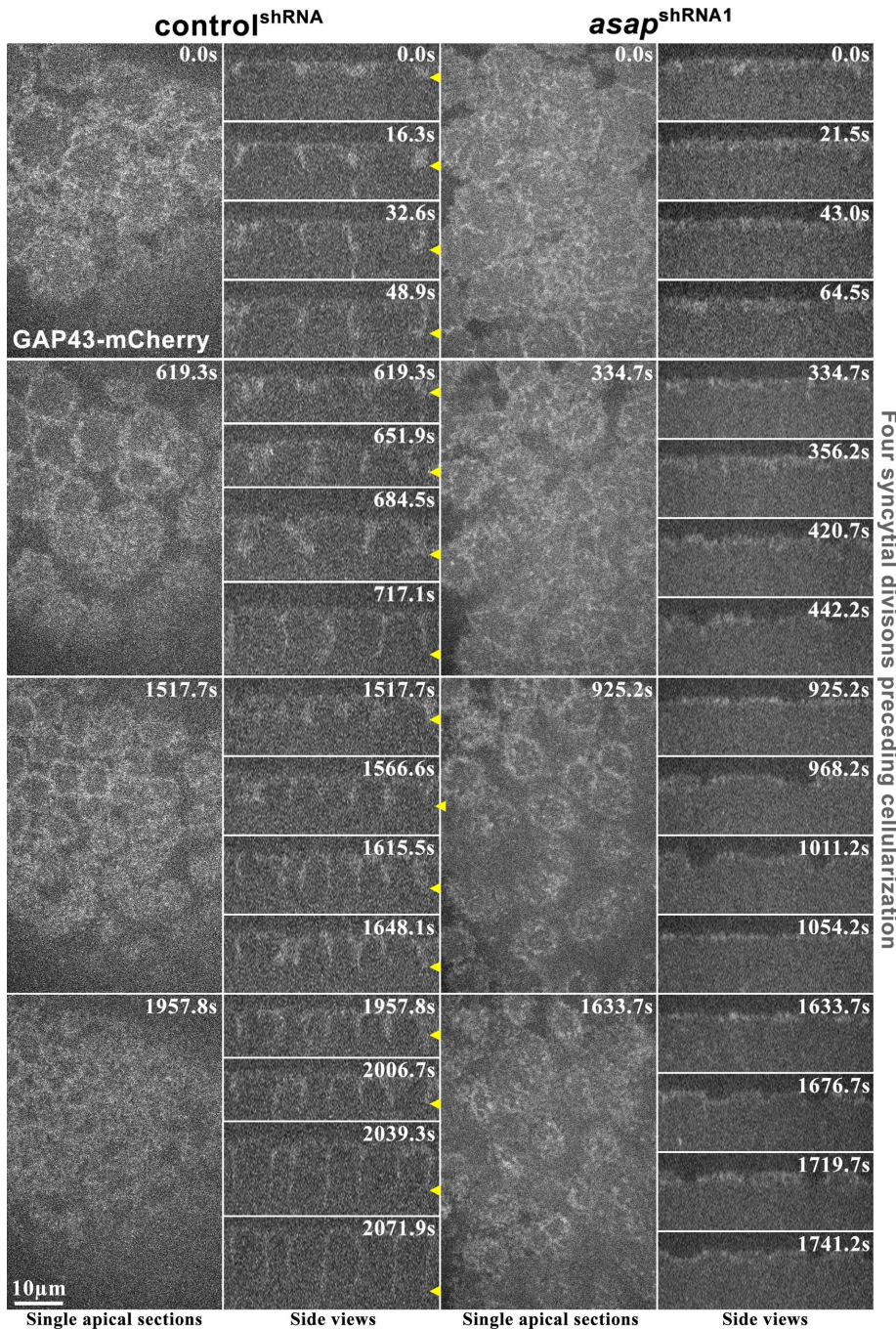


FIGURE 2: *Asap* is necessary for cleavage furrow ingression. Live imaging of the plasma membrane marker GAP43-mCherry during the four cycles of syncytial division preceding cellularization. Apical surface views show the formation of PM caps above nuclei at interphase of each cycle. Side views show the subsequent ingression of furrows from these caps. Caps form with either control or *Asap* RNAi, although caps become more scattered with *Asap* RNAi. Furrows ingress with control RNAi (arrowheads; four of four embryos) but not with *Asap* RNAi (four of six embryos showed no ingression, and two of six embryos showed partial ingression).

Furrow ingression seems largely independent of *Asap* effects on the PM

To distinguish how *Asap* promotes cleavage furrow ingression, we investigated cellular processes affected by *Asap* in other systems known to promote furrow ingression in the early *Drosophila* embryo and implicated by our *Asap* localization analyses. First, we considered the actin cortex. Actin networks stabilize the furrows

(Lee and Harris, 2014), and a PM Arf-GEF, Steppke, has been shown to antagonize these networks to restrain furrow growth (Lee and Harris, 2013). For example, Steppke overexpression weakens furrow actin networks and induces furrow loss through its GEF activity (Lee and Harris, 2013). Thus we hypothesized that *asap* RNAi might eliminate furrows because Steppke was no longer counteracted. To test this hypothesis, we examined whether the effects of *asap* RNAi could be suppressed by *steppke* RNAi through coexpression of shRNA constructs. *steppke* shRNA expression induced abnormal formation of basal membranes (Figure 4A) due to elevated actomyosin activity around the base of the furrows (Lee and Harris, 2013). Double RNAi revealed that the effects of *Asap* depletion were dominant over the effects of Steppke depletion (Figure 4B), suggesting that the *asap* RNAi defects were due to a distinct, and perhaps upstream, dysfunction in furrow formation.

To further examine the possible effect of *Asap* at the PM, we evaluated the first cells formed in the syncytial embryo, the primordial germ cells (PGCs). The furrow formation required for these posterior cells to divide individually from the syncytial soma is also inhibited by abnormally high Steppke GEF activity (Lee et al., 2015b) or loss of actomyosin activity (Cinalli and Lehmann, 2013; Lee et al., 2015b). Strikingly, *asap* RNAi embryos could form PGCs, despite strong furrow disruption in the later soma (Figure 4C; arrows show PGCs). Thus *Asap* seems to promote furrows via a mechanism that is distinct from Steppke and actomyosin regulation and is specifically required in the soma during later peripheral divisions.

Next we considered PM endocytosis, since transcytosis from the apical PM is required for furrow ingression (Pelissier et al., 2003). Consistent with an endocytosis/transcytosis route, disruption of the PM clathrin adaptor complex AP-2 eliminates furrows (Lee and Harris, 2013), as does RNAi of the Golgi and endocytic regulator Arf1 (Lee et al., 2015a). Because the *Asap*-dependent mechanism was specifically required for somatic but not PGC cleavage, we evaluated PGC formation with RNAi of *AP-2α* or *arf1*. RNAi of either

gene resulted in strong furrow disruption in the soma of the syncytial embryo, but only *AP-2α* RNAi disrupted PGC formation (Figure 4C). These results suggest that AP-2-dependent endocytosis is critical for the cleavage of both somatic cells and PGCs, whereas *Asap* and Arf1 are more critical for later cleavage in the soma and thus may contribute mostly to a distinct cellular process.

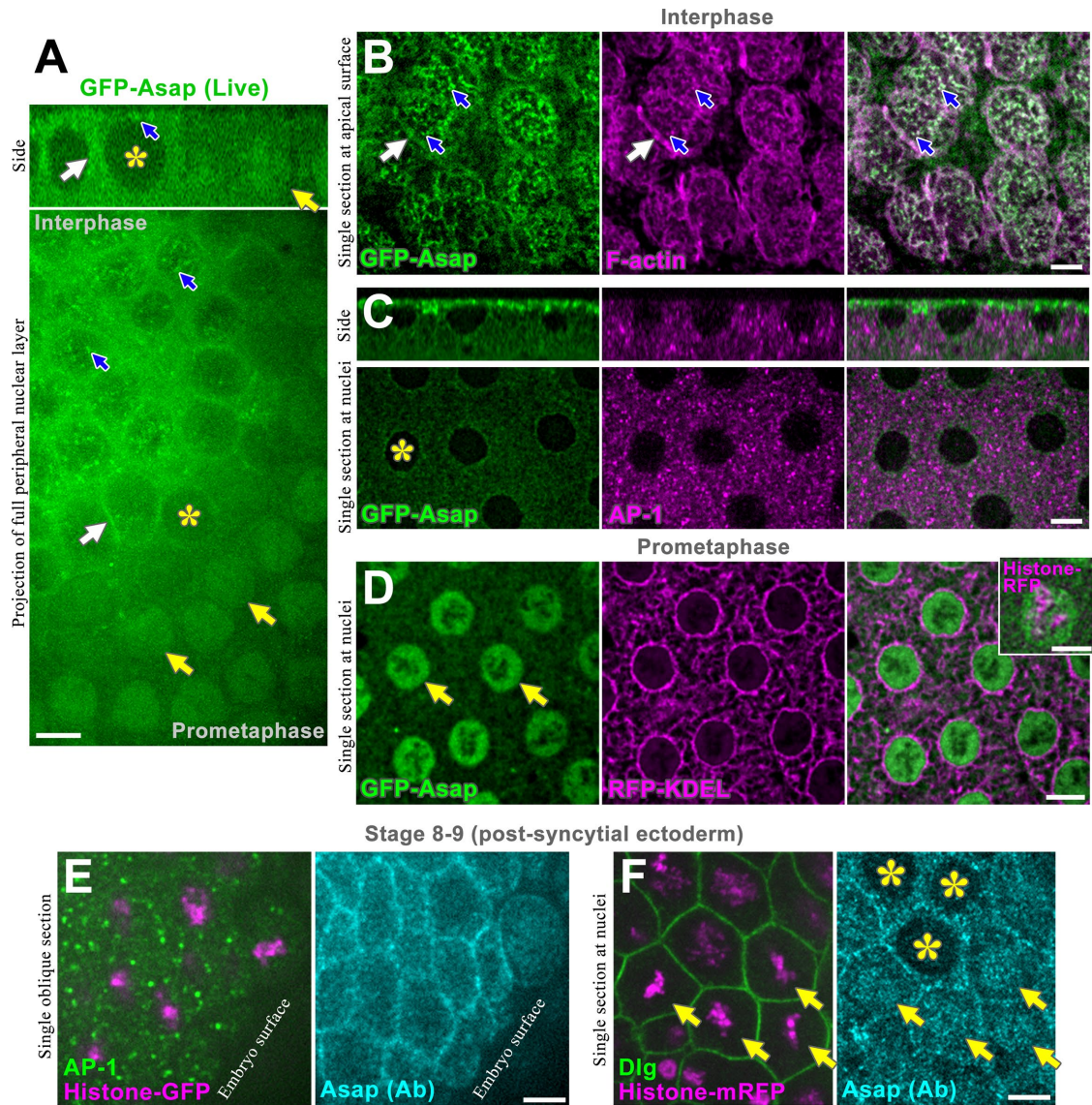


FIGURE 3: Asap localizes to multiple subcellular sites and relocates during the cell cycle. (A) A GFP-Asap-expressing embryo imaged live over a syncytial cell cycle. A side view and a projection of the full peripheral nuclear layer are shown as a mitotic wave spreads across the embryo. At interphase (top left), GFP-Asap is enriched at punctate structures resembling apical microvilli (blue arrows) and at early PM furrows (white arrows) and has a cytoplasmic pool detectable by exclusion from nuclei (yellow asterisks). At the onset of mitosis (bottom right), GFP-Asap is depleted from the PM and becomes enriched at nuclear regions surrounding condensed chromosomes (yellow arrows). After mitosis, GFP-Asap returns to the PM (not shown). (B) Single cross-section at the apical PM surface at interphase. GFP-Asap puncta closely colocalize with F-actin-rich microvilli (arrows). (C) A side view and single section at the nuclear level at interphase shows GFP-Asap most prominently at the PM, more weakly in the cytosol, with slight enrichment around the nuclear periphery, and exclusion from the nucleus. Staining with the Golgi marker AP-1 reveals no enrichment of GFP-Asap at Golgi puncta. (D) GFP-Asap becomes enriched within the nuclear region at prometaphase. RFP-KDEL marks the periphery of the nuclear region. Inset, separation of GFP-Asap from condensed chromosomes (marked with histone RFP). (A–D) Constructs expressed as in Figure 1. (E) Ectoderm of a postsyncytial, stage 8–9 histone-GFP embryo stained for endogenous Asap and the Golgi marker AP-1. The oblique section from the embryo surface (right) inward (left) reveals endogenous Asap strongly at the PM of each cell and weakly in the cytoplasm, with no enrichment at AP-1-positive Golgi elements. (F) Mitotic domain within the ectoderm of a stage 8–9 histone-mRFP embryo stained for endogenous Asap and the PM marker Dlg. At metaphase, endogenous Asap localizes to the nuclear region (yellow arrows) surrounding condensed mitotic chromosomes (histone-mRFP). Endogenous Asap is excluded from the nucleus in interphase cells (yellow asterisks). Bars, 5 μ m.

Asap is required primarily for Golgi organization

Another major contributor to furrow ingression is biosynthetic trafficking from the ER and Golgi (Lecuit and Wieschaus, 2000; Sisson *et al.*, 2000; Frescas *et al.*, 2006; Holly *et al.*, 2015; Mavor

et al., 2016). To probe whether Asap and Arf1 participate in the biosynthetic pathway, we analyzed the Golgi morphology of *asap* RNAi and *arf1* RNAi embryos. In the *Drosophila* early embryo, the Golgi is composed of dispersed tubulovesicular

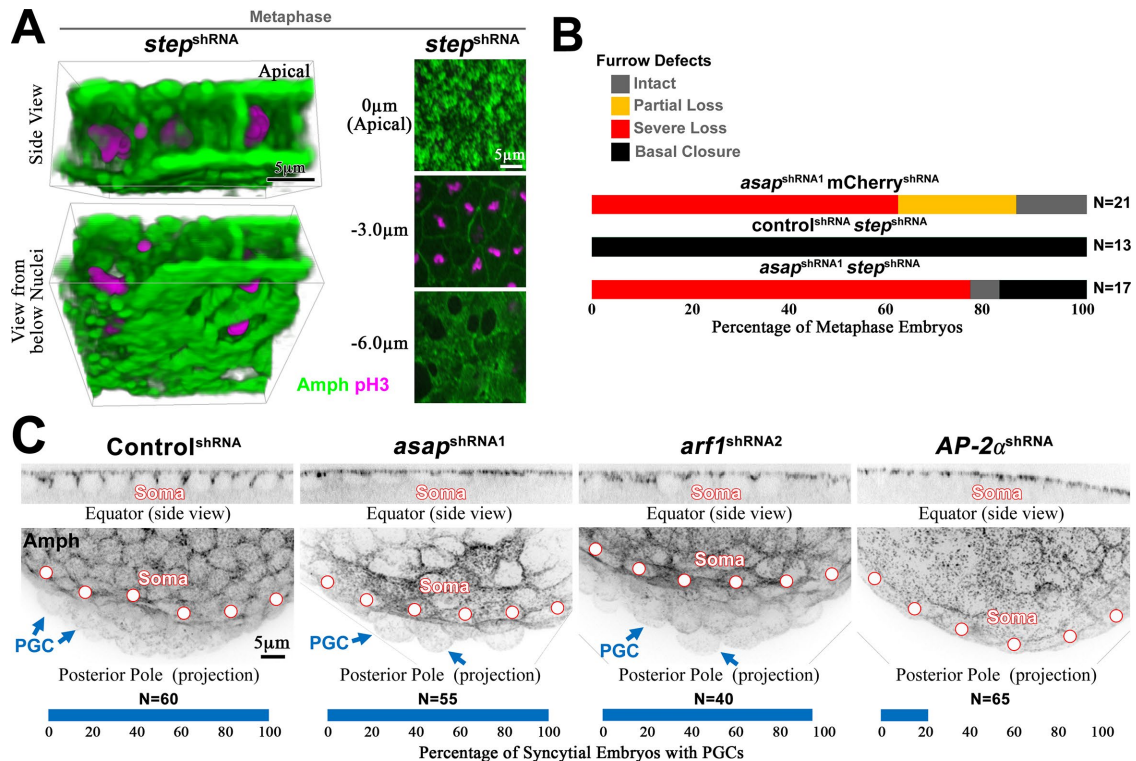


FIGURE 4: Furrow ingression seems independent of possible roles for Asap at the PM. (A) A *steppe^{shRNA}* metaphase embryo with furrow tips expanded to form abnormal basal membranes (shown as a 3D reconstruction of ~10–12 peripheral cell compartments and as xy-sections from the embryo surface to below the nuclei; compare to the shRNA control embryo in Figure 1, B and C). (B) Quantifications of Asap-Steppe and control double RNAi experiments. Note that the furrow loss with Asap RNAi dominates over the furrow tip expansion that otherwise occurs with Steppe RNAi. *N*, number of metaphase embryos counted for each genotype (compiled from two or more experiments, each with similar results). (C) Top, cross-sections of the equatorial somatic region reveal intact furrows with control shRNA and loss of furrows with Asap, Arf1, and AP-2α RNAi (embryos at interphase). Middle, projections of the posterior pole show the formation of PGCs with control, Asap, and Arf1 RNAi but not with AP-2α RNAi. Amphiphysin marks the PM. The PGCs are round and protrude from the posterior pole (arrows). Bottom, quantifications of the presence of PGCs. *N*, embryo numbers (compiled from two or more experiments, each with similar results). Constructs expressed as in Figure 1.

elements that form stacks but lack the ribbon-like organization of other cell types (Ripoche *et al.*, 1994; Rabouille *et al.*, 1999). To probe for Golgi structure, we stained for a *cis*-Golgi marker, GM130 (Lorente-Rodriguez and Barlowe, 2011), and a *trans*-Golgi marker, Liquid facets-related (LqfR; Leventis *et al.*, 2011). In control RNAi embryos, each marker labeled evenly distributed puncta, and GM130 puncta were often adjacent to LqfR puncta (Figure 5). In contrast, both *asap* RNAi and *arf1* RNAi produced abnormal aggregation of Golgi elements, with LqfR-positive structures at the core of the aggregates and GM130 puncta around their periphery (Figure 5). To assess whether this abnormal Golgi morphology occurred in response to general furrow and nuclear disruption, we analyzed the soma of AP-2α RNAi embryos, but these embryos displayed seemingly normal Golgi organization despite severe nuclear disorganization (Figure 5). Moreover, embryos expressing the weaker *asap* shRNA (*asap^{shRNA2}*) displayed moderate Golgi disorganization with normal nuclear organization (Supplemental Figure S3). Thus the main effect of *asap* RNAi seems to be on the Golgi.

Asap promotes Arf1 localization at the Golgi

Because both Asap and Arf1 are required for a similar aspect of Golgi organization, we hypothesized that Asap acts through Arf1 to

control the Golgi. To test this idea, we probed for Arf1 localization using an Arf1-GFP construct that localizes to Golgi puncta (Shao *et al.*, 2010; Lee *et al.*, 2015a; Figure 6A) with dependence on the Golgi Arf GEF Gartenzweg (Armbruster and Luschnig, 2012). In control RNAi embryos at interphase, Arf1-GFP localized strongly to intracellular puncta and also displayed a general cytosolic distribution with nuclear exclusion (Figure 6B). In contrast, strong *asap* RNAi (*asap^{shRNA1}*) depleted all pools of Arf1-GFP, and weaker *asap* RNAi (*asap^{shRNA2}*) did so to a lesser degree (Figure 6, B and D). To assess the specificity of the *asap* RNAi effect, we also probed for Arf4-GFP, which has a distribution similar to that of Arf1-GFP (Lee *et al.*, 2015a; Figure 6C) and found that its levels at the Golgi were increased by *asap* RNAi versus control (Figure 6, C and E). Thus Asap has a specific and essential role in maintaining Arf1 at the Golgi, although it also affects total Arf1 levels through an unknown effect.

To further address how Asap affects the localization of Arf1, we investigated the consequences of Asap overexpression. Specifically, we coexpressed Arf1-GFP with an Asap-mCherry fusion protein or mCherry alone. Compared to the mCherry control, Asap-mCherry overexpression significantly increased Arf1-GFP levels at the Golgi at interphase (Figure 6F). To understand how Asap-mCherry could elevate Arf1-GFP levels at the Golgi, we compared the localization patterns of the proteins at interphase.

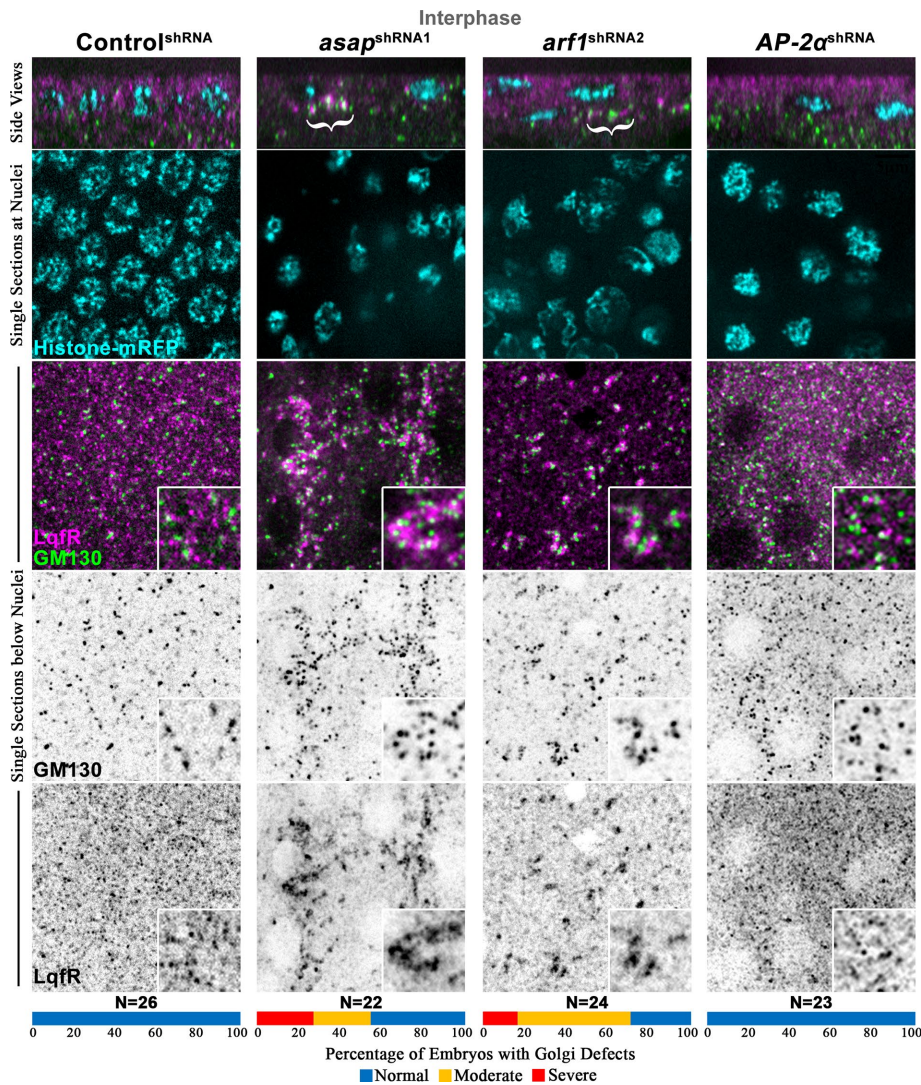


FIGURE 5: *Asap* affects early-embryo Golgi organization. Side views and single cross-sections at or below the nuclei of control, *Asap*, *Arf1*, and *AP-2 α* RNAi embryos expressing histone-mRFP for visualization of nuclei and stained for GM130 and LqfR for markers of the *cis*- and *trans*-Golgi, respectively (embryos at interphase). *cis*- and *trans*-Golgi compartments abnormally aggregate in *Asap* and *Arf1* RNAi embryos (brackets in side views and inserts of single sections). *AP-2 α* RNAi embryos display nuclear disorganization similar to that of *Asap* and *Arf1* RNAi embryos but not the Golgi disorganization. Quantification of Golgi disruptions is presented below. *N*, embryo numbers (compiled from two or more experiments, each with similar results). Constructs expressed as in Figure 1.

Consistent with the localization data of the GFP-tagged *Asap* constructs and the antibody detection of endogenous *Asap* (Figure 3), *Asap*-mCherry localized most prominently to the PM and displayed no enrichment at *Arf1*-GFP-positive Golgi elements (Figure 6G). Intriguingly, *Asap*-mCherry did colocalize with an intermediate pool of *Arf1*-GFP at the PM furrows (Figure 6G, arrows). Together these results indicate that *Asap* is necessary and sufficient for *Arf1* accumulation at the Golgi and may affect *Arf1* at non-Golgi sites.

Asap affects the organization of *Arf1* effectors at the Golgi

To address whether *Asap* affects the activity of endogenous *Arf1* at the Golgi, we examined the localization of two *Arf1* effectors—the COPI coat and the clathrin adaptor AP-1 complex (Lorente-Rodriguez and Barlowe, 2011; Guo *et al.*, 2014; Papanikou and

Glick, 2014). To probe for effects on the COPI coat, we examined a γ COP-GFP construct. In contrast to control RNAi, strong *asap* RNAi or *arf1* RNAi significantly reduced the levels of γ COP-GFP at Golgi puncta, and both perturbations did so to a similar degree (Supplemental Figure S4A). Thus *Asap* and *Arf1* have a common role in promoting COPI coat localization at the Golgi. In contrast, strong *asap* RNAi had no apparent effect on AP-1 γ levels at the Golgi, although AP-1 γ localized to abnormally aggregated Golgi elements (Supplemental Figure S4B), as observed for the other *trans*-Golgi marker, LqfR (Figure 5).

Golgi organization and furrow ingression require an *Arf1*-*Asap* binding site

To test whether *Arf1* is affected by a direct interaction with *Asap*, we generated *Drosophila* versions of two mouse *Arf1* variants shown to be differentially regulated by ASAP1 with in vitro assays of purified *Arf1* and purified *Arf*-GAPs (Luo *et al.*, 2005). Specifically, the GTPase activity of *Arf1*^{L46D} is highly insensitive to activation by ASAP1 and weakly insensitive to activation by AGAP1 or *Arf* GAP1, whereas the GTPase activity of *Arf1*^{N52A} is weakly insensitive to ASAP1, AGAP1, or *Arf* GAP1 (Luo *et al.*, 2005), thus providing a control for effects unrelated to strong *Asap* insensitivity. Because *Drosophila* and mouse *Arf1* have 97% amino acid residue identity and the region of mouse ASAP1 assayed by Luo *et al.* (2005) has 48% amino acid identity with *Drosophila* *Asap*, we generated corresponding *Drosophila* *Arf1* constructs with additional silent mutations for resistance to the *arf1* shRNA. Coexpression of *Arf1*^{N52A} with *arf1* shRNA substantially rescued the cleavage furrow and Golgi defects that otherwise occur with *arf1* RNAi, but coexpression of the *Asap*-insensitive *Arf1*^{L46D} failed to rescue the defects (Figure 7, A and B). Of

note, *arf1* RNAi, like *asap* RNAi, also led to partial female infertility, which was rescued by the *Asap*-sensitive *Arf1* construct but not the *Asap*-insensitive *Arf1* construct (Table 1). Expression of the *Asap*-insensitive *Arf1* construct in an otherwise wild-type background induced female infertility (Table 1), indicating that the transgene does produce an active protein. Overall these data argue that *Asap* acts directly on *Arf1* for Golgi organization and furrow growth in the embryo.

Subtle changes to *Arf1* localization and Golgi structure over the syncytial cell cycle

As mammalian cells enter mitosis, inhibition of Golgi *Arf* GEFs leads to the loss of *Arf1* from the Golgi and Golgi disassembly (Altan-Bonnet *et al.*, 2003). The essential role of *Asap* for *Arf1* function at the Golgi suggests that it could also be a control point, and the

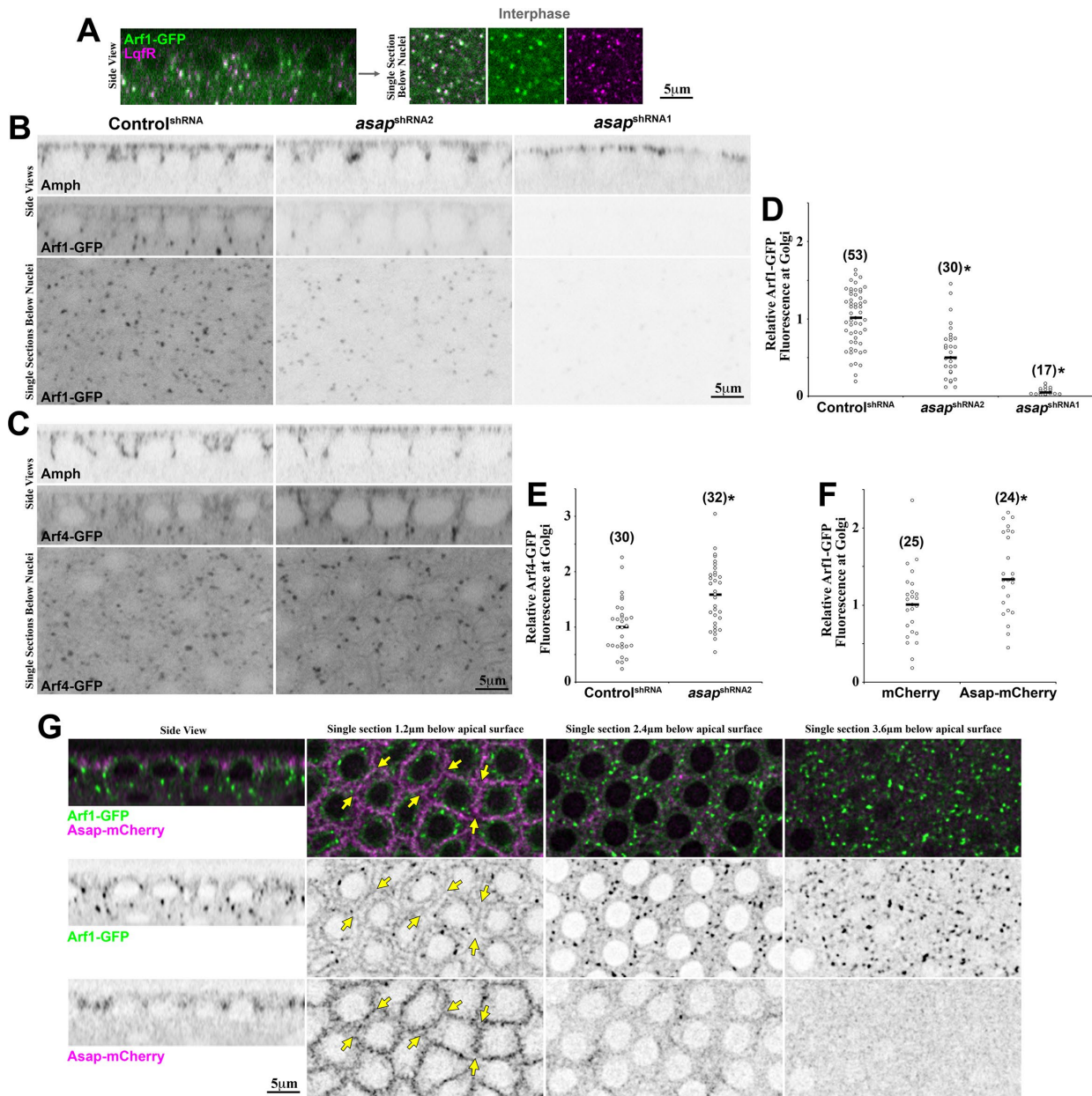


FIGURE 6: Asap is necessary and sufficient for Arf1-GFP accumulation at the Golgi. (A) A syncytial embryo at interphase expressing Arf1-GFP and stained with the Golgi marker LqfR. Note the colocalization of the Arf1-GFP puncta with the Golgi marker. (B) Side views and subnuclear xy-sections of syncytial embryos expressing Control^{shRNA}, asap^{shRNA1}, and asap^{shRNA2} in combination with Arf1-GFP (stained for Amph for staging; embryos at interphase). Images collected and adjusted with the same settings. Note the loss of Arf1-GFP levels at Golgi puncta with Asap RNAi and accompanying general loss of Arf1-GFP. (C) Side views and subnuclear xy-sections of syncytial embryos expressing Control^{shRNA} and asap^{shRNA2} in combination with Arf4-GFP (stained for Amph for staging; embryos at interphase). Images collected and adjusted with the same settings. Note the increase of Arf4-GFP levels at Golgi puncta with Asap RNAi. (D) Quantification of relative Arf1-GFP fluorescence at Golgi puncta for Control^{shRNA}, asap^{shRNA2}, and asap^{shRNA1}. Each dot represents the average levels of one embryo. Black bars indicate median values. Asterisks indicate significant differences ($p < 0.0001$). (E) Quantification of relative Arf4-GFP fluorescence at Golgi puncta for Control^{shRNA} and asap^{shRNA2} as in D. Asterisk indicates significant differences ($p < 0.0001$). (F) Quantification of relative Arf1-GFP fluorescence at Golgi puncta for mCherry and Asap-mCherry-overexpressing embryos as done in D. Asterisk indicates significant differences ($p < 0.0001$). (A–F) Constructs expressed as in Figure 1. (D–F) Data compiled from two or more experiments, each with similar results. (G) Comparison of the localization of Asap-mCherry and Arf1-GFP in a syncytial embryo at interphase. Asap-mCherry localizes most strongly to the PM, with no enrichment at Golgi elements, where Arf1-GFP is most strongly enriched (compare the proteins in the section 3.6 µm below the apical surface). Intermediate pools of Arf1-GFP are found around the nuclear periphery and at the PM (forming concentric circles in the section 1.2 µm below the apical surface). The intermediate pool of Arf1-GFP at the PM colocalizes with Asap-mCherry (arrows). Other than the accumulation difference at Golgi elements, the localization of Arf1-GFP was similar when coexpressed with mCherry (unpublished data).

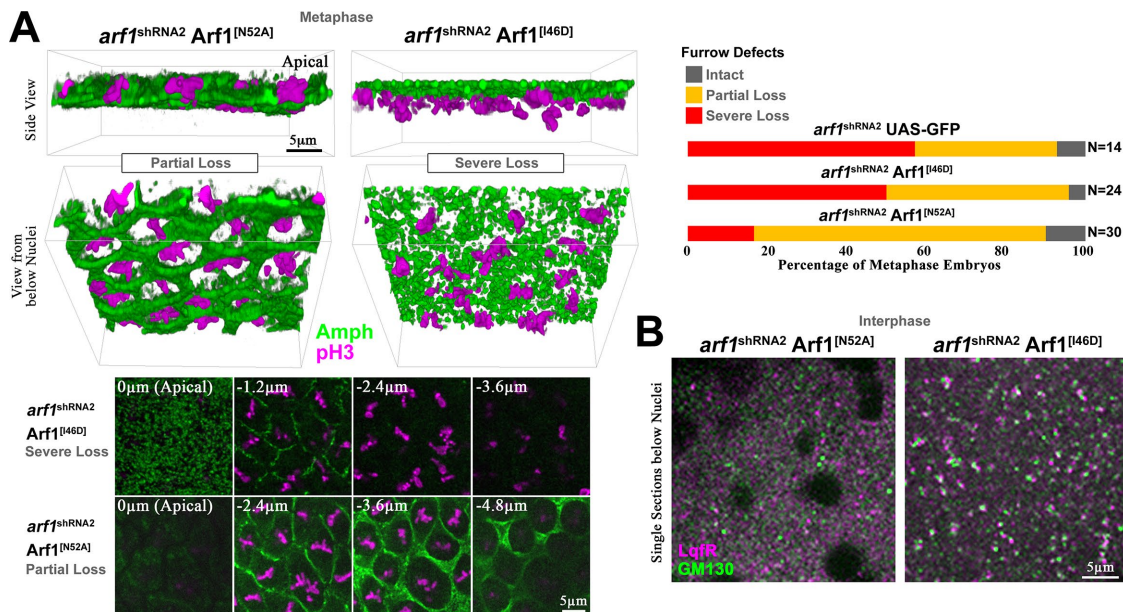


FIGURE 7: An Asap-insensitive Arf1 construct is relatively ineffective for furrow ingression and Golgi organization. (A) 3D reconstructions of metaphase syncytial embryos expressing Arf1 RNAi with RNAi-resistant Arf1^[N52A] (left) or RNAi-resistant Arf1^[I46D] (right). Amph shows furrows, and pH3 shows cell cycle stage. Control Arf1^[N52A] considerably rescues Arf1 RNAi embryos, but Asap-insensitive Arf1^[I46D] does not. Below, *xy*-sections from the embryo surface to below the nuclei. Quantified to the right with Arf1 RNAi embryos coexpressing GFP as a control for the number of UAS constructs. *N*, number of metaphase embryos (compiled from two or more experiments, each with similar results). (B) Single cross-sections below the nuclei of *arf1^{shRNA2} Arf1^[N52A]* (left) and *arf1^{shRNA2} Arf1^[I46D]* (right) embryos stained for GM130 and LqfR (embryos at interphase). More abnormal Golgi aggregation was observed with the Asap-insensitive Arf1^[I46D] than the control Arf1^[N52A]. (A, B) Constructs expressed as in Figure 1.

relocalization of Asap to the nuclear region at mitosis suggests that such control could be cell-cycle regulated. Thus we examined changes to Arf1 and the Golgi over the cell cycle in the early *Drosophila* embryo.

We began by probing for Arf1-GFP localization in fixed tissues with markers of the cell cycle, Golgi, ER, and PM (Figure 8A). At all stages of the cell cycle, strong Arf1-GFP puncta were present and juxtaposed with the *trans*-Golgi marker, LqfR (Figure 8A, single- and double-channel images). However, at metaphase, we observed an increase of Arf1-GFP at both the PM (Figure 8A, blue arrow) and the ER (Figure 8A, yellow arrow, inset, and Supplemental Figure S5), with Arf1-GFP exclusion from the nuclear region (Supplemental Figure S5). These results indicate that both Arf1-Golgi association and Golgi stacking are largely maintained through the cell cycle but that Arf1 partially relocalizes to the PM and ER at metaphase.

For more precise examination of the Arf1-positive Golgi elements, we examined Arf1-GFP live, with coexpressed histone-monomeric red fluorescent protein (mRFP) for staging over the cell cycle. Time-lapse, three-dimensional (3D) analyses of individual embryos revealed that the Arf1-positive Golgi puncta become smaller and more numerous from interphase to metaphase to telophase (Figure 8, B and C). To test whether these changes were due to changes in general Golgi structure, we analyzed fixed embryos stained for the *cis*-Golgi marker GM130 and discovered the same trend (Figure 8C). Thus the Golgi undergoes subtle reorganization over the syncytial cell cycle in *Drosophila*.

DISCUSSION

Our results identify an essential and specific role for Asap in promoting Arf1 activity at the Golgi. Asap promotes Arf1 but not Arf4 localization to the Golgi. Both Asap and Arf1, as well as a conserved

residue responsible for their interaction, are required for proper Golgi structure and the biosynthesis of cleavage furrows. Our genetic analyses argue that the requirements of Asap and Arf1 for furrow ingression are due primarily to effects at the PM. Of note, we also discovered a translocation of Asap to the nuclear region before each cycle of furrow regression and that this change coincides with a transient alteration to Golgi structure, as well as to accumulation of Arf1 at the PM and ER. Overall our data reveal an Asap-Arf1-Golgi pathway for cleavage furrow biosynthesis and that this pathway may be regulated over the cell cycle.

Although we cannot exclude the possibility of Asap acting at the Golgi, the lack of Asap enrichment at Golgi elements suggests that Asap promotes Golgi Arf1 accumulation indirectly, perhaps by recycling the small G protein from other sites. Asap could recycle Arf1 in two ways. First, Asap might inactivate Arf1 to release it from coat proteins (Gillingham and Munro, 2007; Spang *et al.*, 2010; Donaldson and Jackson, 2011; East and Kahn, 2011), thereby resupplying Arf1 after vesicle budding from the Golgi. Second, Asap could function within a kinetic scaffold. This effect increases the supply of GDP-bound G proteins for reaction with GEFs and has been modeled to explain the ability of GAPs to promote the activity of G protein-coupled receptors (Ross, 2008). For Asap, the effect could be coupled with the uncoating of Golgi-derived vesicles or supply Arf1 from more distant membranes (such as the PM, where Asap-Arf1 colocalization is evident).

What is the relationship between Asap and other Arf GAPs that affect Arf1 at the Golgi? mRNA for each of the annotated Golgi Arf GAPs is present in cleavage stage *Drosophila* embryos (FlyBase, <http://flybase.org/>). This expression includes Arf GAPs that affect Arf1 at the Golgi in other systems and do so redundantly for cell

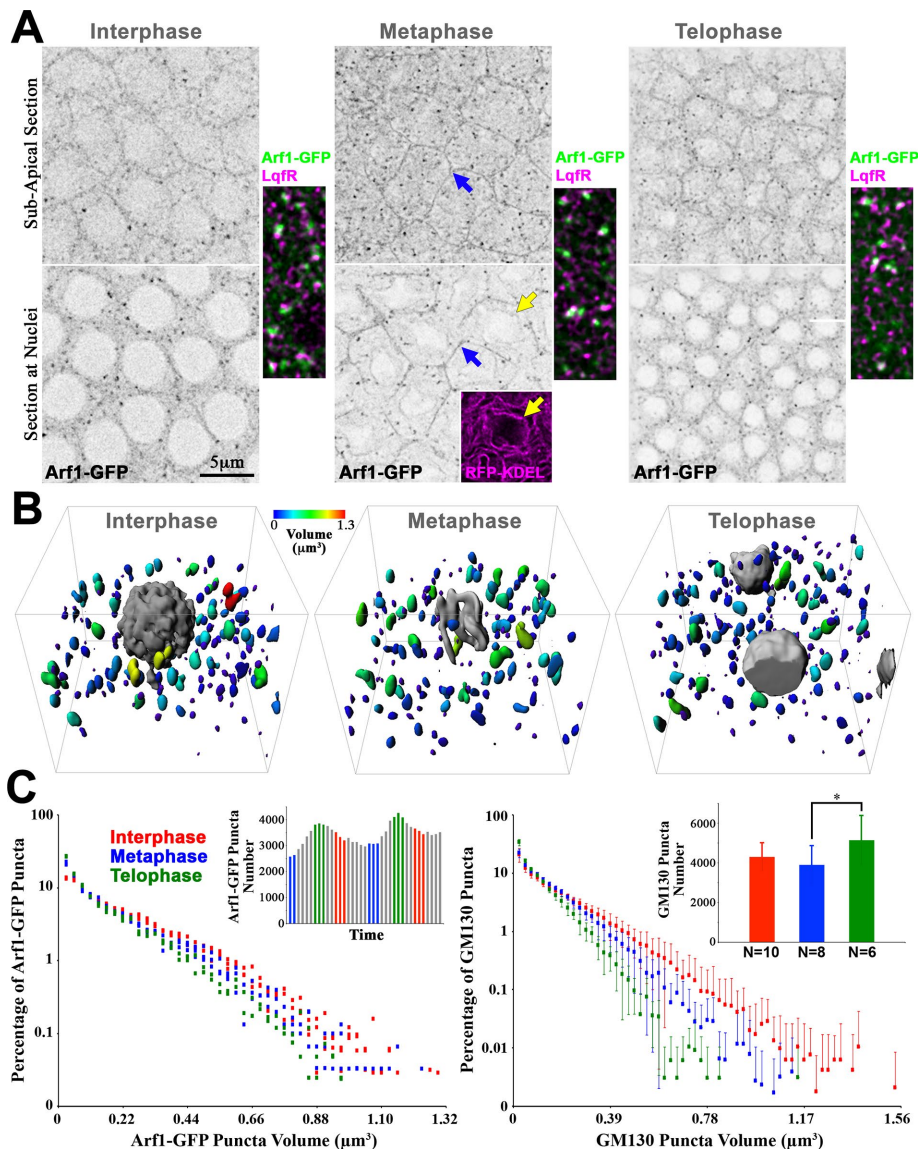


FIGURE 8: Changes to Arf1 localization and Golgi structure over the cell cycle. (A) Single sections of the subapical and nuclear regions of fixed Arf1-GFP-expressing embryos at interphase, metaphase, and telophase. At interphase, Arf1-GFP localizes to Golgi puncta and at the PM to a lesser extent and is excluded from the nucleus. At metaphase, Arf1-GFP increases at the PM (blue arrows) and ER (yellow arrows; inset, RFP-KDEL as a coexpressed ER marker) but is excluded from the spindle region within the ER. By telophase, the Arf1-GFP distribution resembles that at interphase. Side images are single sections below the nuclei of Arf1-GFP embryos at interphase, metaphase, and telophase stained for LqfR to show Golgi ministacks throughout the cell cycle. (B) 3D reconstructions of Arf1-GFP puncta from time-lapse imaging of a single embryo at different stages of the cell cycle. Arf1-GFP puncta are color coded according to volume. (C) Histograms showing Arf1-GFP (left) and GM130 (right) puncta volume distributions at different stages of the cell cycle (color coded). From interphase to telophase, puncta volumes decrease for both Arf1-GFP and GM130. The Arf1-GFP histogram is for time-lapse imaging of a single embryo, and each dot represents the percentage of Arf1-GFP puncta within a volume range (the same trend was observed for three embryos; unpublished data). The GM130 histogram is from imaging of fixed embryos at different cell cycle stages, and each dot represents a mean \pm SD of the percentage of GM130 puncta within a volume range for the embryo at that cell cycle stage (embryo numbers in inset). Insets quantify total numbers of puncta per cell cycle stage (color coded). For Arf1-GFP, each bar represents one time frame (30 s/time frame) from time-lapse imaging of one embryo (the same trend was observed for three embryos), and for GM130, the bars show means \pm SD. An increase in total puncta number was evident for both Arf1-GFP and GM130 ($*p < 0.05$). N, embryo numbers (compiled from two or more experiments, each with similar results). (A–C) Constructs expressed as in Figure 1.

viability (Gillingham and Munro, 2007; Spang *et al.*, 2010; Donaldson and Jackson, 2011; East and Kahn, 2011). Because Asap's promotion of Arf1 at the Golgi seems essential for cleavage furrow formation, its specific mechanism of action may be unique, perhaps due to the larger complexes it forms and/or to the subcellular location where it acts.

How does mitotic Golgi reorganization compare among different systems? Mitosis of mammalian cells involves strong loss of Golgi Arf1 (Altan-Bonnet *et al.*, 2003), disassembly of Golgi ribbons (Altan-Bonnet *et al.*, 2003), and destacking of Golgi elements (Lucocq *et al.*, 1989; Misteli and Warren, 1995; Zaal *et al.*, 1999). Such disassembly may allow Golgi membranes to partition evenly between daughter cells, and, in addition, loss of Arf1 leads to release of cytoskeletal regulators from the Golgi for roles in furrow formation (Altan-Bonnet *et al.*, 2003). In the early *Drosophila* embryo, mitotic changes to Golgi organization seem quite distinct. First, extended Golgi ribbons are never present, and at each cell cycle stage, the Golgi exists as numerous ministacks that would presumably partition evenly to daughter compartments. Second, Arf1 only partially redistributes from the Golgi at metaphase (to the ER and PM), and only subtle changes to Golgi elements are detected (to their sizes and numbers). Third, this metaphase Golgi reorganization is followed by cleavage furrow regression rather than ingression. There may also be a major regulatory difference between these systems. Specifically, the Arf1 loss in mammalian cells is primarily due to reduced Arf GEF activity (Altan-Bonnet *et al.*, 2003). In contrast, we speculate that the relocalization of Asap to the nuclear region at prometaphase could reduce both Arf1 function at the Golgi and the biosynthesis of furrows. Although definition of the nuclear localization mechanism is required for understanding this or other effects at mitosis, sequestration of an Arf GAP, rather than loss of an Arf GEF, could allow subtle Golgi regulation for cycles of furrow regression in rapid succession with extensive furrow growth. Significantly, furrow regression could also involve sequestration of other players, as nonmuscle myosin II relocalizes to the nuclear region at mitosis (Lee and Harris, 2013), as does dynamin (Rikhy *et al.*, 2015). Perhaps sequestration of several factors temporarily halts the fuelling and maintenance of cleavage furrows for these natural cycles of furrow regression.

Overall our results show that Asap is essential for Arf1 to function at the Golgi for cleavage furrow biosynthesis. Asap may

recycle Arf1 to the Golgi from post-Golgi membranes, providing optimal Golgi output for specific stages of the cell cycle.

MATERIALS AND METHODS

Drosophila stocks and genetics

Established stocks. The following fly lines were used: maternal- α -tubulin-GAL4::VP16 (gift of M. Peifer, University of North Carolina, Chapel Hill, NC), Maternal Triple Driver (MTD; Bloomington *Drosophila* Stock Center [BDSC], stock 31777), UASp-mCherry-shRNA (P[VALIUM20-mCherry]attP2, BDSC, stock 35785), UASp-GFP-Asap, UASp-Arf1-GFP (Shao *et al.*, 2010), UASp-Arf4-GFP (Lee *et al.*, 2015a), UASp-*arf1*-shRNA2 (Lee *et al.*, 2015a), UASp-RFP-KDEL (BDSC, stock 30910), UASp-yCOP-GFP (BDSC, stock 29711), Histone2Av-mRFP1 (BDSC, stock 23650), histone-GFP (gift of A. Wilde, University of Toronto, Toronto, Canada), and GAP-43-mCherry (gift of S. Simoes, University of Toronto). UASp-Asap-GFP and UASp-Asap-mCherry were generated as UASp-GFP-Asap (Shao *et al.*, 2010), with the exception of destination vectors for C-terminal GFP or mCherry tagging.

asap shRNA constructs. The shRNAs were designed based on the algorithm by Vert *et al.* (2006). For *asap1*, they targeted two unique sequences: shRNA1 top strand, 5'-ctagcagtTAAG-TTCAGCGTTGTCACCAAtagttatattcaagcataTTGGTGACAAC-GCTGAACCTTAGcg-3'; and shRNA2 top strand, 5'-ctagcagtA-AGACTGTGATCCGATATGTatagttatattcaagcataTACATATCG-GATCACAGTCTTgcg-3'. The control shRNA construct targeted the top strand sequence 5'-ctagcagtCCGAGTGTGTTCTGATCCTAtagttatattcaagcataTAGGATCAGAAACACACTC-GGgcg-3'. The *asap1* shRNA1 and control shRNA constructs were ligated into the pValium22 vector, and the *asap1* shRNA2 construct was ligated into the pValium20 vector (gifts from the Transgenic RNAi Resource Project, www.flyrnai.org/TRiP-HOME.html/), using the restriction enzymes *NheI* and *EcoRI*, confirmed by PCR, sequenced, and targeted to the *atp40* recombination site on chromosome 2 for transgenic flies (BestGene, Chino Hills, CA).

RNAi-resistant Arf1 constructs. Gene synthesis (GenScript Biotech, Piscataway, NJ) produced the nucleotide sequence of the *arf79f* cDNA (LD24904) flanked by *NotI* and *XbaI* restriction sites (5'-GCGGCCGC[TTTGGCAGCA...TTTAATTTTT]TCTAGA-3') with the shRNA target region mutated from 5'-CTGAGGGATGCAGTCT-TACTA-3' to 5'-TTACGTGACGCCGTACTCTTG-3' (maintaining the encoded protein sequence) and mutations to produce the amino acid change I46D or N52A. The vector was cut by *NotI* and *XbaI* and cloned into the pUASp-attB vector (with no protein tag). The vectors were inserted into the genome at the *atp2* recombination site on the third chromosome for transgenic flies (BestGene).

Crosses. For UAS transgene expression in the early embryo, we analyzed progeny of mothers heterozygous for maternal- α -tubulin-GAL4::VP16 or MTD and for the transgene.

Embryo staining and imaging

Embryos were fixed for 20 min in 1:1 3.7% formaldehyde in phosphate-buffered saline (PBS):heptane and then devitellinized in methanol. Blocking and staining were in PBS containing 1% goat serum, 0.1% Triton X-100, and 1% sodium azide. Antibodies used were as follows: rabbit, amphiphysin (1:2000; gift of G. Boulianne, Hospital for Sick Children, Toronto, Canada), Asap (1:500; gift of R. Johnson, Wesleyan University, Middletown, CT), and GM130 (1:700;

Abcam, Cambridge, United Kingdom); mouse, AP-1 γ (1:500; gift of R. Le Borgne, University of Rennes, Rennes, France), Dlg (1:100; Developmental Studies Hybridoma Bank [DSHB]), and phospho-histone H3 (1:2000; Cell Signaling Technology, Beverly, MA); and rat, LqfR (1:500; gift of G. Boulianne). Secondary antibodies were conjugated to Alexa Fluor 488, 568, and 647 (Life Technologies, Burlington, Canada). Embryos were mounted in Aqua Polymount (Polysciences, Warrington, PA).

For tubulin and actin staining, embryos were washed with 0.1% Triton X-100, dechorionated with 50% bleach, washed with 0.1% Triton X-100, fixed for 10 min in 1:1 10% formaldehyde in PBS:heptane, devitellinized by hand peeling, and stained. Tubulin was stained with mouse anti-tubulin (E7; 1:100; DSHB). F-actin was stained with Alexa Fluor 568-conjugated phalloidin (1:200; Life Technologies).

For live imaging, dechorionated embryos were glued to a coverslip using tape adhesive dissolved in heptane and mounted in halocarbon oil (series 700; Halocarbon Products, River Edge, NJ). The coverslip, with the embryos facing up, was set into the bottom of a glass-bottom culture dish with its original coverslip removed.

Immunofluorescence images were collected by a spinning-disk confocal system (Quorum Technologies, Guelph, Canada) at room temperature using 40 \times Plan Neofluar numerical aperture (NA) 1.3 and 63 \times Plan Apochromat NA 1.4 objectives (Carl Zeiss, Toronto, Canada) with a piezo top plate and a Hamamatsu C9100-13 electron-multiplying charge-coupled device camera (Hamamatsu Photonics, Hamamatsu, Japan), with z-stacks of 1- μ m and 300-nm step sizes for the 40 \times and 63 \times objectives, respectively.

Postacquisition image analyses and quantification

Basic image analysis and preparation. Images were analyzed with Volocity software (PerkinElmer, Waltham, MA). Photoshop (Adobe, Mountain View, CA) was used for figure preparation. Except where noted, input levels were adjusted so the main signal range spanned the entire output grayscale. Images were resized by bicubic interpolation without noticeable changes at normal viewing magnifications.

Quantifications of Golgi Arf1-GFP and Arf4-GFP levels. For each embryo, ImageJ (National Institutes of Health, Bethesda, MD) was used to measure mean fluorescence intensity of the GFP signal within a circle with a diameter of 0.6 μ m covering each of five puncta most strongly stained with the Golgi marker LqfR. When the raw fluorescence signal was too weak to be clearly seen by the naked eye, deconvolved and adjusted images of the LqfR staining indicated the position of the Golgi to measure the raw Arf1-GFP signal at these sites (the Arf1-GFP data were not manipulated before the quantification). Background values were measured within the nuclear region nearest to the Golgi measurement and subtracted from the Golgi measurements individually. For each embryo, these corrected values were then averaged to calculate a single fluorescence intensity measurement, which was then plotted and compared with those of other embryos.

Quantification of furrow defects. Syncytial embryos were staged at metaphase by chromosome morphology seen by phospho-histone H3 staining. Only embryos in cell cycle 11, 12, or 13 were analyzed. Cycle 10 embryos were excluded by nuclear density. Embryos with ≤ 50 nuclei per field of view (65.3 μ m [x] \times 65.3 μ m [y]) were discarded. Furrow integrity was analyzed with Amph staining. Embryos with nuclei completely surrounded by ingressing furrows

were categorized as having intact cleavage furrows. Embryos with nuclei that were only partially enclosed by furrows were categorized as having partial furrow defects. Embryos in which >50% of nuclei did not have any ingressed furrows surrounding them were categorized as having severe furrow defects. Only somatic nuclei at the equator of the embryo were imaged for analysis.

Three-dimensional surface rendering of Golgi puncta. Imapris 6.2 software (Bitplane AG, Zurich, Switzerland) was used for 3D surface rendering of Arf1-GFP and GM130 puncta. Parameters were optimized such that 3D surfaces closely resembled the raw data by eye. Data sets for time points of Arf1-GFP live imaging were quantified with a volume of 65.3 (x) × 65.3 (y) × 18 μm (z), including the full peripheral cell compartments. Data sets for the fixed GM130 images were quantified with a volume of 65.3 (x) × 65.3 (y) × 6 μm (z) just below the nuclei of the peripheral cell compartments.

Statistics. Comparisons were done using Student's *t* tests (independent samples, two-tailed). Means are shown with SDs. Scatterplots prepared with an available template (Weissgerber *et al.*, 2015).

ACKNOWLEDGMENTS

We thank Sergey Plotnikov and Andrew Wilde for critiquing the manuscript and Gabrielle Boulianne, Ruth Johnson, Roland Le Borgne, Mark Peifer, Sergio Simoes, Andrew Wilde, and the *Drosophila* Transgenic RNAi Resource Project for reagents. The work was supported by Canadian Institutes of Health Research Operating Grant MOP82829 to T.H., who was also supported by a Tier 2 Canada Research Chair.

REFERENCES

Altan-Bonnet N, Phair RD, Polishchuk RS, Weigert R, Lippincott-Schwartz J (2003). A role for Arf1 in mitotic Golgi disassembly, chromosome segregation, and cytokinesis. *Proc Natl Acad Sci USA* 100, 13314–13319.

Armbruster K, Luschnig S (2012). The *Drosophila* Sec7 domain guanine nucleotide exchange factor protein Gartzweg localizes at the cis-Golgi and is essential for epithelial tube expansion. *J Cell Sci* 125, 1318–1328.

Bharti S, Inoue H, Bharti K, Hirsch DS, Nie Z, Yoon HY, Artym V, Yamada KM, Mueller SC, Barr VA, *et al.* (2007). Src-dependent phosphorylation of ASAP1 regulates podosomes. *Mol Cell Biol* 27, 8271–8283.

Cinalli RM, Lehmann R (2013). A spindle-independent cleavage pathway controls germ cell formation in *Drosophila*. *Nat Cell Biol* 15, 839–845.

Donaldson JG, Jackson CL (2011). ARF family G proteins and their regulators: roles in membrane transport, development and disease. *Nat Rev Mol Cell Biol* 12, 362–375.

East MP, Kahn RA (2011). Models for the functions of Arf GAPs. *Semin Cell Dev Biol* 22, 3–9.

Foe VE, Alberts BM (1983). Studies of nuclear and cytoplasmic behaviour during the five mitotic cycles that precede gastrulation in *Drosophila* embryogenesis. *J Cell Sci* 61, 31–70.

Frescas D, Mavrikis M, Lorenz H, Delotto R, Lippincott-Schwartz J (2006). The secretory membrane system in the *Drosophila* syncytial blastoderm embryo exists as functionally compartmentalized units around individual nuclei. *J Cell Biol* 173, 219–230.

Frigerio G, Grimsey N, Dale M, Majoul I, Duden R (2007). Two human ARFGAPs associated with COP-I-coated vesicles. *Traffic* 8, 1644–1655.

Frolov MV, Alatorsev VE (2001). Molecular analysis of novel *Drosophila* gene, Gap69C, encoding a homolog of ADP-ribosylation factor GTPase-activating protein. *DNA Cell Biol* 20, 107–113.

Furman C, Short SM, Subramanian RR, Zetter BR, Roberts TM (2002). DEF-1/ASAP1 is a GTPase-activating protein (GAP) for ARF1 that enhances cell motility through a GAP-dependent mechanism. *J Biol Chem* 277, 7962–7969.

Gillingham AK, Munro S (2007). The small G proteins of the Arf family and their regulators. *Annu Rev Cell Dev Biol* 23, 579–611.

Guo Y, Sirkis DW, Schekman R (2014). Protein sorting at the trans-Golgi network. *Annu Rev Cell Dev Biol* 30, 169–206.

Holly RM, Mavor LM, Zuo Z, Blankenship JT (2015). A rapid, membrane-dependent pathway directs furrow formation through RalA in the early *Drosophila* embryo. *Development* 142, 2316–2328.

Johnson RI, Sedgwick A, D'Souza-Schorey C, Cagan RL (2011). Role for a Cindr-Arf6 axis in patterning emerging epithelia. *Mol Biol Cell* 22, 4513–4526.

Lecuit T (2004). Junctions and vesicular trafficking during *Drosophila* cellularization. *J Cell Sci* 117, 3427–3433.

Lecuit T, Wieschaus E (2000). Polarized insertion of new membrane from a cytoplasmic reservoir during cleavage of the *Drosophila* embryo. *J Cell Biol* 150, 849–860.

Lee DM, Harris TJ (2013). An Arf-GEF regulates antagonism between endocytosis and the cytoskeleton for *Drosophila* blastoderm development. *Curr Biol* 23, 2110–2120.

Lee DM, Harris TJ (2014). Coordinating the cytoskeleton and endocytosis for regulated plasma membrane growth in the early embryo. *Bioarchitecture* 4, 68–74.

Lee DM, Rodrigues FF, Yu CG, Swan M, Harris TJ (2015a). PH domain-Arf G protein interactions localize the Arf-GEF Steppke for cleavage furrow regulation in *Drosophila*. *PLoS One* 10, e0142562.

Lee DM, Wilk R, Hu J, Krause HM, Harris TJ (2015b). Germ cell segregation from the *Drosophila* soma is controlled by an inhibitory threshold set by the Arf-GEF Steppke. *Genetics* 200, 863–872.

Leventis PA, Da Sylva TR, Rajwans N, Wasiake S, McPherson PS, Boulianne GL (2011). Liquid facets-related (lqfR) is required for egg chamber morphogenesis during *Drosophila* oogenesis. *PLoS One* 6, e25466.

Liu Y, Yerushalmi GM, Grigera PR, Parsons JT (2005). Mislocalization or reduced expression of Arf GTPase-activating protein ASAP1 inhibits cell spreading and migration by influencing Arf1 GTPase cycling. *J Biol Chem* 280, 8884–8892.

Lorente-Rodriguez A, Barlowe C (2011). Entry and exit mechanisms at the cis-face of the Golgi complex. *Cold Spring Harb Perspect Biol* 3, a005207.

Lucocq JM, Berger EG, Warren G (1989). Mitotic Golgi fragments in HeLa cells and their role in the reassembly pathway. *J Cell Biol* 109, 463–474.

Luo R, Jacques K, Ahvazi B, Stauffer S, Premont RT, Randazzo PA (2005). Mutational analysis of the Arf1*GTP/Arf GAP interface reveals an Arf1 mutant that selectively affects the Arf GAP ASAP1. *Curr Biol* 15, 2164–2169.

Mavor LM, Miao H, Zuo Z, Holly RM, Xie Y, Loerke D, Blankenship JT (2016). Rab8 directs furrow ingression and membrane addition during epithelial formation in *Drosophila melanogaster*. *Development* 143, 892–903.

Mazelova J, Astuto-Gribble L, Inoue H, Tam BM, Schonteich E, Prekeris R, Moritz OL, Randazzo PA, Deretic D (2009). Ciliary targeting motif VxPx directs assembly of a trafficking module through Arf4. *EMBO J* 28, 183–192.

Mazumdar A, Mazumdar M (2002). How one becomes many: blastoderm cellularization in *Drosophila melanogaster*. *Bioessays* 24, 1012–1022.

Min MK, Jang M, Lee M, Lee J, Song K, Lee Y, Choi KY, Robinson DG, Hwang I (2013). Recruitment of Arf1-GDP to Golgi by Glo3p-type ArfGAPs is crucial for golgi maintenance and plant growth. *Plant Physiol* 161, 676–691.

Misteli T, Warren G (1995). Mitotic disassembly of the Golgi apparatus in vivo. *J Cell Sci* 108, 2715–2727.

Papanikou E, Glick BS (2014). Golgi compartmentation and identity. *Curr Opin Cell Biol* 29, 74–81.

Pelissier A, Chauvin JP, Lecuit T (2003). Trafficking through Rab11 endosomes is required for cellularization during *Drosophila* embryogenesis. *Curr Biol* 13, 1848–1857.

Poon PP, Cassel D, Spang A, Rotman M, Pick E, Singer RA, Johnston GC (1999). Retrograde transport from the yeast Golgi is mediated by two ARF GAP proteins with overlapping function. *EMBO J* 18, 555–564.

Rabouille C, Kuntz DA, Lockyer A, Watson R, Signorelli T, Rose DR, van den Heuvel M, Roberts DB (1999). The *Drosophila* GMII gene encodes a Golgi alpha-mannosidase II. *J Cell Sci* 112, 3319–3330.

Randazzo PA, Andrade J, Miura K, Brown MT, Long YQ, Stauffer S, Roller P, Cooper JA (2000). The Arf GTPase-activating protein ASAP1 regulates the actin cytoskeleton. *Proc Natl Acad Sci USA* 97, 4011–4016.

- Rikhy R, Mavrikis M, Lippincott-Schwartz J (2015). Dynamin regulates metaphase furrow formation and plasma membrane compartmentalization in the syncytial *Drosophila* embryo. *Biol Open* 4, 301–311.
- Ripoche J, Link B, Yucel JK, Tokuyasu K, Malhotra V (1994). Location of Golgi membranes with reference to dividing nuclei in syncytial *Drosophila* embryos. *Proc Natl Acad Sci USA* 91, 1878–1882.
- Ross EM (2008). Coordinating speed and amplitude in G-protein signaling. *Curr Biol* 18, R777–R783.
- Shao W, Wu J, Chen J, Lee DM, Tishkina A, Harris TJC (2010). A modifier screen for Bazooka/PAR-3 interacting genes in the *Drosophila* embryo epithelium. *PLoS One* 5, e9938.
- Sisson JC, Field C, Ventura R, Royou A, Sullivan W (2000). Lava lamp, a novel peripheral golgi protein, is required for *Drosophila melanogaster* cellularization. *J Cell Biol* 151, 905–918.
- Sisson JC, Rothwell WF, Sullivan W (1999). Cytokinesis: lessons from rappaport and the *Drosophila* blastoderm embryo. *Cell Biol Int* 23, 871–876.
- Spang A, Shiba Y, Randazzo PA (2010). Arf GAPs: gatekeepers of vesicle generation. *FEBS Lett* 584, 2646–2651.
- Sullivan W, Theurkauf WE (1995). The cytoskeleton and morphogenesis of the early *Drosophila* embryo. *Curr Opin Cell Biol* 7, 18–22.
- Trieselmann N, Wilde A (2002). Ran localizes around the microtubule spindle in vivo during mitosis in *Drosophila* embryos. *Curr Biol* 12, 1124–1129.
- Vert JP, Foveau N, Lajaunie C, Vandenbrouck Y (2006). An accurate and interpretable model for siRNA efficacy prediction. *BMC Bioinformatics* 7, 520.
- Walker DL, Wang D, Jin Y, Rath U, Wang Y, Johansen J, Johansen KM (2000). Skeletor, a novel chromosomal protein that redistributes during mitosis provides evidence for the formation of a spindle matrix. *J Cell Biol* 151, 1401–1412.
- Wang J, Morita Y, Mazelova J, Deretic D (2012). The Arf GAP ASAP1 provides a platform to regulate Arf4- and Rab11-Rab8-mediated ciliary receptor targeting. *EMBO J* 31, 4057–4071.
- Weissgerber TL, Milic NM, Winham SJ, Garovic VD (2015). Beyond bar and line graphs: time for a new data presentation paradigm. *PLoS Biol* 13, e1002128.
- Zaal KJ, Smith CL, Polishchuk RS, Altan N, Cole NB, Ellenberg J, Hirschberg K, Presley JF, Roberts TH, Siggia E, et al. (1999). Golgi membranes are absorbed into and reemerge from the ER during mitosis. *Cell* 99, 589–601.